Ultrafast photoexcitation dynamics in a ladder-type oligophenyl

C. Gadermaier,* G. Cerullo, M. Zavelani-Rossi, G. Sansone, and G. Lanzani
Dipartimento di Fisica, Politecnico di Milano, P.zza Leonardo da Vinci 32, 20133 Milano, Italy

E. Zojer and A. Pogantsch
Inst. f. Festkörperphysik, Technische Universität Graz, Petersgasse 16, 8010 Graz, Austria

D. Beljonne
Service de Chimie des Matériaux Nouveaux, Centre de Recherche en Electronique et Photonique Moléculaires, Université de Mons-Hainaut, Place du Parc 20, B 7000 Mons, Belgium

Z. Shuai
Center for Molecular Science, Institute of Chemistry, The Chinese Academy of Science, Beijing 100080, People's Republic of China

J. L. Brédas
Department of Chemistry, The University of Arizona, Tucson, Arizona 85721-0041

U. Scherf
Institut f. Physikalische Chemie u. Theoretische Chemie, Universität Potsdam, Kârl-Liebknecht-Str. 24-25, D-14476 Golm, Germany

G. Leising
Science & Technology, AT&S AG, Fabriksgasse 13, 8700 Leoben, Austria
(Received 4 February 2002; published 11 September 2002)

Sub-ps transient differential transmission spectroscopy is used to study the photoexcitation dynamics of a blue emitting ladder-type oligophenyl in bulk film. The observed spectral features are ascribed to singlet excited states and polarons. The time traces of these features reveal the dynamics of charge-carrier generation from singlets via a migration-assisted dissociation mechanism.

DOI: 10.1103/PhysRevB.66.125203 PACS number(s): 78.47.+p, 42.65.Re, 36.20.Kd, 31.25.Qm

I. INTRODUCTION

Conjugated organic materials are currently experiencing the dawn of their commercialization in electroluminescent and photovoltaic devices. Recently, an electrically pumped laser has been realized by using an organic conjugated molecular single crystal.[1] The physics of conjugated systems is under investigation since the early days of quantum mechanics[2] and the understanding of fundamental properties has constantly backed the achievements in practical applications. At this point a rather comprehensive background for discussing the optical and electrical properties has been established, however, some critical issues are still left unclear.

Time resolved spectroscopy is a powerful tool for investigating elementary excitation dynamics, and it has contributed significantly to the definition of the fundamental photophysics of conjugated materials. Numerous ultrafast studies have identified the electronic transition from the first excited singlet state[3] $S_1$to the ground state S_0 as the origin of stimulated emission (SE) in solutions[4,5] and solid films[6–8] of conjugated polymers. A transition from the S_1 state to a higher excited singlet state S_n has been associated with the broad photoinduced absorption (PA) band which appears around energies lower than the S_0-S_1 transition. In methyl-substituted ladder-type poly(para)phenylene (*m*-LPPP),[6] this band peaks at 1.5 eV. The PA dynamics over a broad range of wavelengths, however, indicates a contribution by electronic transitions from a species other than S_1, which has been ascribed to polarons,[6] created as loosely bound pairs from the S_1 state. The interplay between neutral charged and neutral states in conjugated materials is not fully understood.

A successful strategy for gaining insight into the photophysics of these materials is the use of model compounds, which are prototypes displaying all the fundamental characteristics of their class in addition to particular ease in both sample preparation and measurement. Since *m*-LPPP is one of the best-characterized conjugated polymers and the most promising candidate for a polymer laser in the blue-turquoise region,[9,10] we chose a five-ring oligomer of analogous chemical structure (5LOPP, Fig. 1) as a model compound.

In the present paper we report on transient spectroscopy investigations of thin films of 5LOPP. Transmission difference spectra and their dynamics allow us to extract a detailed picture of the photoexcitation process, pointing out interchain relaxation as a mechanism for charge generation.

II. EXPERIMENTAL AND THEORETICAL METHODOLOGY

A. Experimental

5LOPP films of thickness approximately 100 nm were spin coated upon glass substrates from solution in Cl-benzene. A frequency-doubled Ti-sapphire laser system with chirped-pulse amplification (CPA) produced the pump

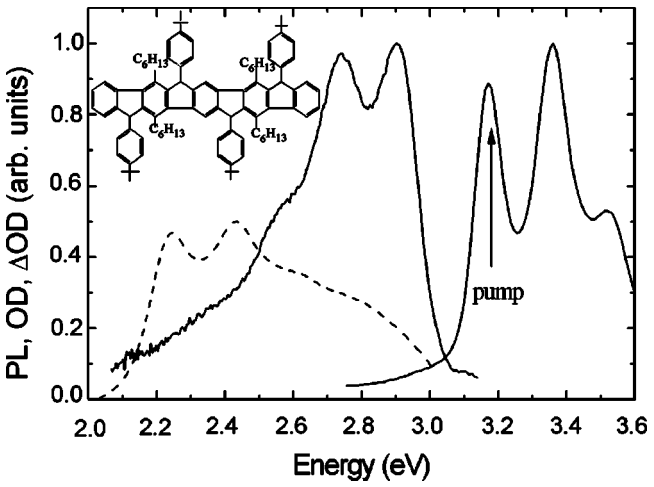

FIG. 1. Photoluminescence and absorption (solid) and doping-induced absorption (dashed) spectra of 5LOPP. Inset shows the chemical structure of 5LOPP.

pulses, with a duration of approximately 150 fs. The probe pulses, covering the 400–900-nm spectral region, were obtained by white light generation in a thin sapphire plate and focused onto the pumped region of the sample via spherical mirrors, to reduce dispersion-induced pulse chirping. The pump pulse was focused onto a spot of 60 μm in diameter via a spherical lens. To reduce photodegradation during the measurements the samples are kept at a vacuum of less than 10^{-3} mbar. The signals are picked up by a an Oriel MS125 spectrograph coupled to a charge-coupled device (CCD) spectrometer Instaspec4 for recording spectra at fixed pump-probe delay, or via a photodiode preceded by an interference filter (bandwidth 10 nm) for measuring the temporal dynamics in selected spectral regions. The cw absorption and doping-induced absorption measurements were performed in a Perkin-Elmer Lambda 9 spectrometer on a 5LOPP film on a glass substrate, drop cast from a solution in chloroform doped with nitrosil-tetrafluorborate. The cw photoluminescence spectra were taken with a Shimadzu RF5301PC spectrofluorophotometer.

B. Theoretical

In order to identify features related to excited-state absorption processes, we have performed correlated quantum-chemical calculations. The time scales of our experiments are much longer than those involved in the lattice relaxation processes following the absorption of the pump beam. Therefore, to simulate excited state absorption processes, one has to consider transitions from molecules in their relaxed excited-state geometry. To evaluate these geometries, we have coupled the semiempirical Hartree-Fock Austin model 1 (AM1) Hamiltonian[11] to a multielectron configuration interaction (MECI) scheme, as implemented in the AMPAC program package.[12] Since the AM1 approach has been parametrized to reproduce ground-state geometries without a post Hartree-Fock treatment, the semiempirical parameters implicitly contain electron correlation effects. Therefore care has to be taken when selecting the CI active space, in order to avoid an overestimation of the electronic correlation in the excited states. Studies on the excited state lifetimes of bridged and nonbridged oligophenylenes[13] indicate that the best description of the geometry of the first singlet excited state in these materials can be achieved by including only excitations from the highest occupied molecular orbital (HOMO) to the lowest unoccupied molecular orbital (LUMO) in the CI procedure.[14]

On the basis of these AM1-MEC1 optimized geometries, the transition energies and oscillator strengths describing the excited-state absorption processes are calculated with the intermediate neglect of differential overlap (INDO) Hamiltonian,[15] coupled either to a multireference determinant single and double configuration interaction technique (MRD-CI),[16] or a single and double equation of motion approach (SD-EOM).[17] The combined AM1/MECI +INDO/MRD-CI approach has already been used in previous studies to successfully explain excited-state absorption processes in zinc porphyrins.[18] However, in contrast to SD-EOM, the MRD-CI formalism is not size consistent. Therefore, although the more elaborated MRD-CI scheme is likely to provide more accurate results in short molecules, the SD-EOM chain-length dependence of the excited-state properties is expected to be more reliable.

III. RESULTS

A. Time-integrated absorption and emission spectra

Absorption and emission spectra of 5LOPP films at room temperature are shown in Fig. 1 together with the chemical structure of the molecule. Both display well resolved spectral features suggesting a vibronic progression with an energy spacing of 0.2 eV. The apparent Stokes shift between the absorption and emission peak, of about 0.2 eV, hints towards an excitation energy relaxation mechanism whose nature will be elucidated by our time-resolved studies.

B. Transient differential transmission spectra

The transmission difference spectrum ($\Delta T/T$) of 5LOPP films photoexcited at 3.18 eV, i.e., in resonance with the first absorption peak, is shown in Fig. 2 for different delays after excitation. An increased transmission ($\Delta T/T>0$) is observed at energies above 2.5 eV and is assigned to stimulated emission (SE) because of the vanishing ground-state absorption in that spectral region; it has the same spectral shape and peak positions as fluorescence, including its vibronic structure. For energies lower than 2.5 eV, there is a broad photoinduced absorption (PA) band peaking at 1.8 eV. This band contains weak features at higher energies (at approximately 2.4, 2.2, and 2.0 eV), and a hump at the lower energy side peaking at roughly 1.5 eV. For longer pump-probe delays, the whole spectrum decays with a small modification of the peak shape, which becomes more evident when probing the dynamics at selected wavelengths. To ease the following discussion, we give a common label to the features with the same dynamics, thus using PA_1 for the 1.5, 1.8, and 2.0 eV features and PA_2 for the humps at 2.2 and 2.4 eV.

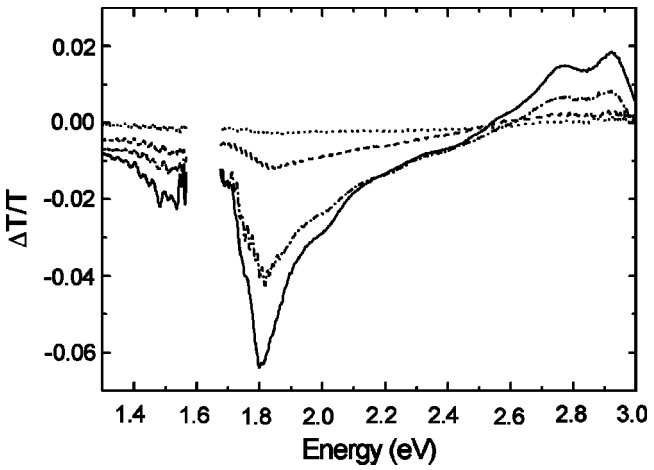

FIG. 2. Transient photoinduced transmission spectra for pump-probe delays of 500 fs (solid), 2 ps (dash-dot), 20 ps (dash), and 200 ps (dot).

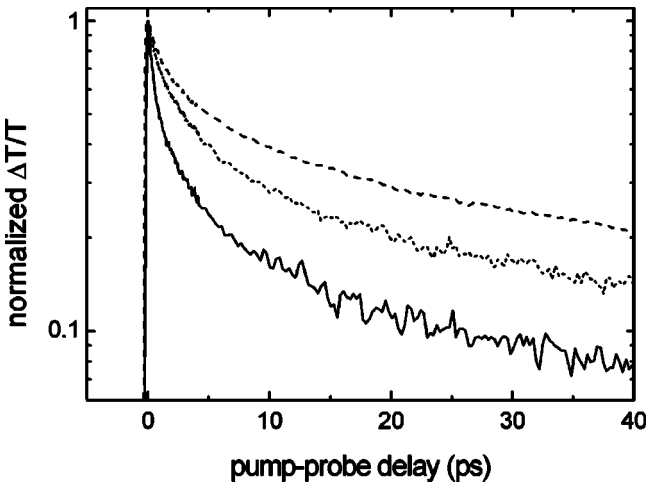

FIG. 3. Temporal evolution of $\Delta T/T$ at 2.8 eV (solid), 2.2 eV (dash), and 1.8 eV (dot).

From SE, it is possible to calculate the gain cross section σ_S, which is an essential parameter for laser applications. For $\Delta T/T \ll 1$, the gain cross section can be related to the differential transmission:

$$\frac{\Delta T}{T} = \exp(\sigma_S n_S d) - 1 \approx \sigma_S n_S d \tag{1}$$

with n_S the number of singlet excitons per cm^3 and d the light path in the gain medium, i.e., the sample thickness. Assuming that each absorbed photon creates one singlet exciton, for short enough pump-probe delays (no significant decay), an upper limit for n_S can be worked out as

$$n_s \leqslant \frac{E(1-10^{-\mathrm{OD}})}{h\nu A d} \tag{2}$$

with E the pulse energy, OD the optical density of the sample, $h\nu$ the photon energy, and A the irradiated area. For the spectrum in Fig. 2, which has been recorded at a pulse energy of 80 nJ (excitation density 1.6×10^{20} cm^{-3}), $\Delta T/T = 1.6\%$ at 2.8 eV and thus $\sigma_S = 8\times10^{-18}$ cm^2. This is almost one order of magnitude lower than in *m*-LPPP.[19] However, two observations should be put forward: (i) As becomes clear when comparing Figs. 1 and 3, the fluorescence of 5LOPP extends far beyond the gain region of the $\Delta T/T$ spectrum, hence there is an appreciable competition between gain and loss due to photoinduced absorption. (ii) As will be pointed out below, there is a fast generation of photoexcited states other than singlet excitons. Therefore not all of the singlet excitons originally created in the sample can contribute to SE. The value obtained from the measured gain is thus to be considered as a lower limit of the actual gain cross section of the $S_1 \rightarrow S_0$ transition.

C. Differential transmission dynamics

Figure 3 shows the transient behavior of SE, PA_1, and PA_2 at an excitation density of 8×10^{19} cm^{-3}. The SE has been recorded at the 2.8-eV peak, PA_1 at the 1.8-eV peak, and PA_2 at 2.2 eV. During the first 15 ps, all three features display a clearly nonexponential decay with SE being the fastest and PA_2 the slowest. After 15 ps, the behavior is approaching a more exponential decay. The dynamics of SE and PA_1 show a strong dependence on the excitation density, which is less accentuated for PA_2. This is shown by the transient behavior at the short timescale depicted in Fig. 4. The difference in the behavior of the two signatures is concentrated on the short pump-probe delays. Note that the density of absorbing ground states is approximately 10^{21} cm^{-3}. The excitation density n_S calculated via Eq. (2) can therefore be overestimated due to saturation effects for the higher pump intensity, while saturation should be negligible for all other data. In this case a significant bleaching lowers the optical density OD and the actual n_S can be lower than the calculated value. This means that the ratio between the two n_S values is actually lower, which leads to an underestimation of the annihilation parameter γ_0 in the fit below.

D. Identification of the transient absorption features

In Fig. 1 the dashed line shows the change in absorption upon chemical doping (doping induced absorption, DIA) of 5LOPP. The spectrum contains two peaks from radical cations at 2.4 and 2.2 eV, which correspond exactly to the PA_2 peaks. We assign the 2.2-eV peak to the transition from the polaron ground state to an excited polaron state, and the 2.4-eV peak to a vibronic replica of this transition (the energy spacing between the two peaks is again approximately 0.2 eV, as is found for PL and ground-state absorption; the transition energy is 0.3 eV higher than in *m*-LPPP,[5] which is consistent with the higher energies found as well for the S_1-S_n absorptions and the cw features).

The photogeneration dynamics of such charged states, taking place within the first few ps after excitation, is discussed below. They represent a small fraction of the initial excited-state population because the $\Delta T/T$ signal is weak and their absorption cross section is expected to be of the same order of magnitude as that of S_1. This is consistent

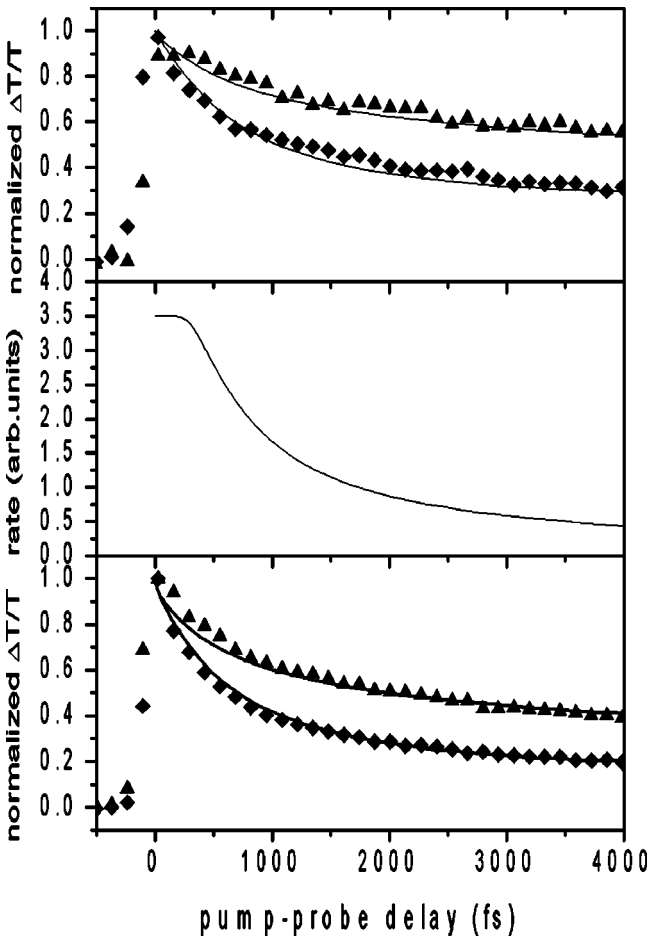

FIG. 4. SE (diamonds) and PA_1 (triangles) dynamics at 8×10^{19} (upper) and 4×10^{20} cm^{-3} (lower graph). The middle graph shows the transient behavior of $k_S^*(t)$ (see text).

with the fact that in general the generation of charged states is not the main excitation pathway for conjugated materials in the solid state.

To identify the transitions originating from the S_1 state (i.e., excited-state absorption), we have performed INDO/MRDCI and INDO/SD-EOM calculations. The results are summarized in Table I.[20] Both methods fully reproduce the three-peak structure found for the PA_1 features, i.e., a large oscillator strength is found for the $S_1\rightarrow S_8$ (S_{10}), $S_1\rightarrow S_{12}$ (S_{13}), and $S_1\rightarrow S_{14}$ (S_{14}) transitions at the MRD-CI (SD-EOM) level. The transition energies for the excited-state absorption process are slightly overestimated by the MRD-CI approach (by approximately 0.2 eV) while SD-EOM tends to underestimate these energies (by about the same amount). For the emission process ($S_1\rightarrow S_0$ transition at the relaxed geometry), the deviation is somewhat bigger (0.5 eV) at the MRD-CI level and amounts to only 0.2 eV for SD-EOM; both approaches therefore appear as useful techniques to describe with a reasonable accuracy both ground-state and excited-state absorption. The lowest-lying excited state displays a marked single-particle character, i.e., its CI description is dominated by a determinant in which a single electron has been promoted from the HOMO to the LUMO. In contrast, all states reached via excited-state absorption display a highly correlated nature, as can be deduced from the large number of contributing excited determinants with relatively similar weights. The nature of the excited states that are coupled through large transition moments to the S_1 state will be discussed elsewhere[21]

The temporal evolution of the differential transmission spectrum (Fig. 2) includes the possibility of a further long-lived species with a broad peak around 2.0 eV, since the 1.8-eV feature shifts slightly to the blue and becomes broader on the high-energy side. Quantum chemical calculations predict a triplet at 2.0 eV.[22] However, since this absorption feature overlaps with both the singlet and polaron absorptions, no time trace that reasonably reflects the triplet population dynamics can be extracted.

IV. DISCUSSION

From the results described in the previous section, we can sketch a picture of the excitation kinetics in the system. Absorption of pump photons at 3.2 eV populates the lowest-lying electronic state (S_1), which is dipole allowed in 5LOPP. Its transient spectral signatures are the induced optical transitions from S_1, responsible for PA_1 (peaks at 1.5, 1.8, and 2.0 eV) and SE (2.5–3.0 eV), respectively. The structures within PA_1, given the common decay, can be assigned to optical transitions from S_1 reaching different higher-lying (even-parity) electronic states. In fact, our calculations yield three relevant transitions to higher singlet states S_n in the range 1.0–2.0 eV. SE and PA_1 consistently

TABLE I. Transition energies, oscillator strengths and most prominent CI expansion coefficients for the transition between the ground and the lowest one-photon allowed state ($S_1\rightarrow S_0$: emission) and for the dominant excited-state absorption processes ($S_1\rightarrow S_8$, $S_1\rightarrow S_{12}$, and $S_1\rightarrow S_{14}$). The oscillator strengths are given relative to that of the $S_1\rightarrow S_0$ transition. All calculations have been performed for the relaxed S_1 geometry (Ref. 20).

Transition		Energy (eV)		Relat. Osc. Strength	
MRD-CI	SD-EOM	MRD-CI	SD-EOM	MRD-CI	SD-EOM
$S_1\rightarrow S_0$	$S_1\rightarrow S_0$	3.35	3.05	1	1
$S_1\rightarrow S_8$	$S_1\rightarrow S_{10}$	1.68	1.30	0.24	0.08
$S_1\rightarrow S_{12}$	$S_1\rightarrow S_{13}$	1.94	1.66	1.23	0.84
$S_1\rightarrow S_{14}$	$S_1\rightarrow S_{14}$	2.28	1.83	0.44	0.37

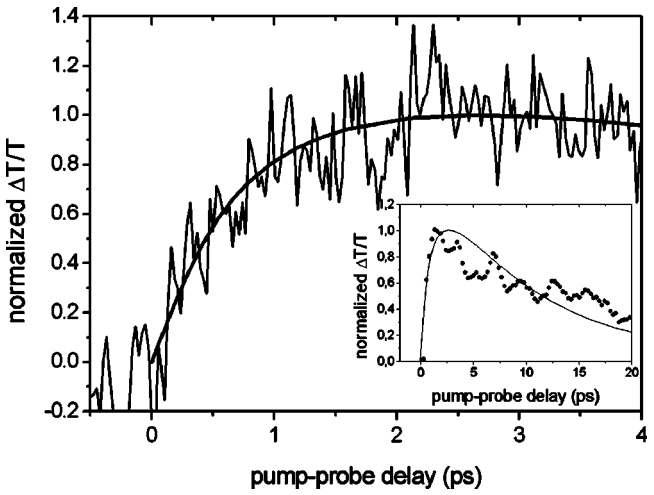

FIG. 5. Difference between normalized $\Delta T/T$ traces at 2.2 and 1.8 eV. The thick line shows the calculated polaron population. The inset shows the same dynamics on a longer time scale.

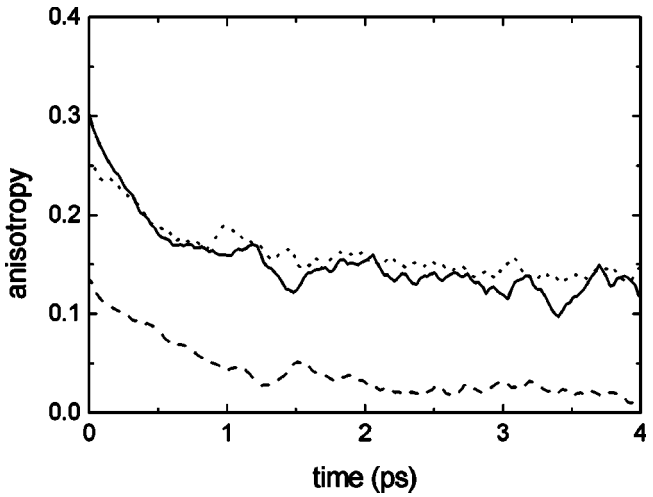

FIG. 6. Anisotropy of differential transmission at 2.8 eV (solid), 2.2 eV (dash), and 1.8 eV (dot).

display roughly the same temporal evolution when observed on the long time scale (>15 ps). The blue shift of the zero-crossing photon energy with time in Fig. 2 indicates that PA_2 is longer lived than SE and hence originates, at least in part, from a different species, which we identified as the polaron. At the spectral position of PA_2 there is, however, an overlap between the absorption of both singlets and polarons. The two components can be partially untangled by a subtraction of the normalized PA_1 and PA_2 time traces, which is depicted in Fig. 5. The polarons are forming on a time scale of a few ps. If the formation rate were constant it would at some point be compensated by the polaron decay and the curve would remain horizontal. Instead, after the maximum is reached, the curve decays again. This leads to the conclusion that the formation rate is decreasing with time or that the charge generation mechanism is active only during a few ps after excitation. Note that in subtracting the two normalized time traces we do not consider charges which are eventually generated during the pump pulse, either from singlets created at a dissociation site or via a sequential excitation mechanism as proposed by Silva *et al.*[23] Hence the curves in Fig. 5 represent only the fraction of the polarons which are not directly created.

The transient polarization memory loss in disordered materials generally indicates migration of the excited state between randomly oriented molecules. Figure 6 depicts the transient behavior of the anisotropy ρ, which is defined as

$$\rho = \frac{(\Delta T/T)_{\text{parallel}} - (\Delta T/T)_{\text{perpendicular}}}{(\Delta T/T)_{\text{parallel}} + 2(\Delta T/T)_{\text{perpendicular}}}. \tag{3}$$

The indices parallel and perpendicular indicate the relative polarization of the pump and probe beams. The factor 2 in the denominator comes from the fact that in Cartesian coordinates, where there is one axis parallel to the original polarization, two axes are perpendicular, but only one of them can be probed in the experiment.

The polarization of the S_1 state, represented by the anisotropy time traces of SE and PA_1, shows a rapid decay during the first ps after excitation, from a value slightly below the theoretical maximum of $\rho = 0.4$ (the initial difference between the two time traces is not significant within the experimental uncertainty) to a ρ value around 0.15, whereafter the decay slows down significantly. From this behavior we deduce a migration of at least a fraction the S_1 states on the ps time scale. PA_2 involves contributions from both S_1 and polaron states. The lower anisotropy compared to PA_1 suggests that the polaron component shows little or no polarization at all.

The previous description and assignments should be refined, if we consider the discrepancy between the kinetics of PA_1 and SE observed at short pump-probe time delays (Fig. 4). PA_1 has a slower decay and less pronounced intensity dependence compared to SE. This is a rather puzzling result. If both features represented the pure S_1 state kinetics, the two time traces would have to be exactly the same. The simple explanation we propose for rationalizing the results and to complete our picture is spectral overlap in the SE region with some strong PA transition, due to new excitations "X." If the generation and/or decay dynamics of the X state is slower than that of S_1, the contribution of this PA to the overall ΔT signal leads to a faster apparent SE decay. In order to support our interpretation, we performed numerical simulations based on the following rate equations for pulsed excitation:

$$\frac{dS}{dt} = -\gamma(t)S^2 - k_S^*(t)S - k_S S, \tag{4}$$

$$\frac{dX}{dt} = k_S^*(t)S_1 - k_X X, \tag{5}$$

where S is the population density of the S_1 states, $\gamma(t)$ is their time dependent bimolecular recombination rate with $\gamma(t) = \gamma_0 \text{erf}(t^{-1/2}) \sim \gamma_0 t^{-1/2}$, $k_S^*(t)$, and k_S are unimolecular singlet decay rates. X is the population density of the state whose PA overlaps with SE and k_X its decay rate. $\gamma(t)$ is written for a non-Markovian process driven by dipole-dipole

coupling within a disordered ensemble.[24] k_S is the singlet decay rate which comprises all unimolecular processes except the formation of the X state, which is given by the time-dependent generation rate $k_S^*(t)$. We note that a bimolecular generation process of the X state as a product of singlet annihilation was first attempted in the simulation, but was unsuccessful. The population kinetics are compared to the ΔT signal using $\Delta T/T(2.8\ \mathrm{eV}) = \sigma_{1-0} S_1 - \sigma_x X d$ and $\Delta T/T(1.8\ \mathrm{eV}) = \sigma_{1-n} S_1 d$. Here d is the effective thickness to be considered and σ_{1-0}, σ_{1-n}, and σ_x are the transition cross sections for SE, singlet PA, and X-state PA, respectively.

In order to reproduce correctly the excitation density dependence we needed a bimolecular singlet annihilation process, plus a unimolecular mechanism with a rate constant $k_S^*(t)$, which becomes negligible within the same time scale of interchain thermalization, as shown in Fig. 4. We chose a transient behavior of this process as described by a power-law decay, $k_S^*(t) = K_S^*(0)\mathrm{erf}(t^{-\alpha}) \propto K_S^*(0) t^{-\alpha}$ representing a process fading off in time, since the difference in the dynamics between SE and PA_1 is evident only for the first few ps after excitation. Reasonably good fitting of the kinetics could be obtained by using the following set of parameters: $\gamma_0 = 1\times10^{-23}\ \mathrm{cm^3\ fs^{-1}}$; $K_S^*(0) = 3.5\times10^{-4}\ \mathrm{fs^{-1}} = (2.8\ \mathrm{ps})^{-1}$; $\alpha = 1$; $k_X = 1.5\times10^{-4}\ \mathrm{fs^{-1}}$ (6.7 ps); $k_{S=}10^{-6}\ \mathrm{fs^{-1}}$ (1 ns), $\sigma_{1-0} = \sigma_{x=}\sigma_{1-n}$. In our model, $k_S^*(t)$ represents the generation rate of the state X from hot singlets during interchain migration. The model suggests the generation of a short-lived species ($1/k_X \approx 7$ ps) during singlet exciton migration, which absorbs in the spectral region where we probed SE. The moving singlet reaches a dissociating site, likely a pair of adjacent oligomers where charge separation is energetically favored, or a photo-oxidized site which traps an electron. Hence it is tempting to conjecture that X be a charged state. In fact, calculating the transient X population from our model provides a behavior which *strikingly matches the polaron population dynamics* [see Fig. 5 which compares the X dynamics obtained from the fit of the SE time trace using Eqs. (4) and (5) with the normalized difference between the measured PA_1 and PA_2 time traces] is found; this corroborates the assignment of the X species to polarons. Additional support comes from the DIA spectrum shown in Fig. 1, which extends well into the SE region. We recall that the proposed mechanism via dissociating sites encountered during migration does not exclude that there is also charge generation within the pump duration, either directly from a singlet created at a dissociating site or via a sequential mechanism as proposed by Silva *et al.*[23] The dynamics of this part of the charge population is not represented in either of the curves of Fig. 5.

V. CONCLUSION

We have presented a comprehensive study of the ultrafast photoexcitation dynamics in 5LOPP. The various PA features (one of which is hidden beneath the SE and causes the SE transient behavior to differ from that of the S_1-S_n absorption) were attributed to S_1 and polaron states. A distribution of site energies in the bulk film drives interchain relaxation. In the course of this migration excitons can dissociate and form polarons. We quantitatively described the S_1 decay channels—unimolecular decay, bimolecular annihilation, and migration-assisted dissociation—as well as polaron formation (from S_1 dissociation) and decay. The obtained population dynamics are in excellent agreement with the experimental results for different excitation densities.

ACKNOWLEDGMENTS

We wish to thank C. Zenz, F. P. Wenzl, S. Stagira, E. J. W. List, and R. Resel (x ray of films) for fruitful discussions as well as P. Malgarise, E. Pettinari, and L. Ligabue for their contribution to the pump-probe experiments. C.G. thanks the TMR-EUROLED project for a research grant. The work at Arizona is partly supported by the National Science Foundation (CHEM-0078819), the IBM Shared University Research program, and the Petroleum Research Fund. E.Z. and A.P. acknowledge financial support by the Spezialforschungsbereich Elektroaktive Stoffe.

*Corresponding author. Fax: +39-02-2399-6126; email address: gadermai@fubphpc.tu-graz.ac.at

[1] J. H. Schön, Ch. Kloc, A. Dodalapur, and B. Batlogg, Science **289**, 599 (2000).
[2] A. J. Heeger, S. Kivelson, J. R. Schrieffer, and W.-P. Su, Rev. Mod. Phys. **60**, 781 (1988).
[3] L. Salem, *The Molecular Theory of Conjugated Systems* (W. A. Benjamin, Reading, MA, 1966), p. 359.
[4] W. Graupner, G. Leising, G. Lanzani, M. Nisoli, S. De Silvestri, and U. Scherf, Chem. Phys. Lett. **246**, 95 (1995).
[5] M. Yan, L. J. Rothberg, E. W. Kwock, and T. M. Miller, Phys. Rev. Lett. **75**, 1992 (1995).
[6] W. Graupner, G. Lanzani, G. Leising, M. Nisoli, S. De Silvestri, and U. Scherf, Phys. Rev. Lett. **76**, 847 (1996).
[7] G. J. Denton, N. Tessler, N. T. Harrison, and R. H. Friend, Phys. Rev. Lett. **78**, 733 (1997).
[8] P. A. Lane, S. V. Frolov, and Z. V. Vardeny, in *Semiconducting Polymers*, edited by G. Hadziioannou and P. F. van Hutten (Wiley-VCH, Weinheim, 2000), p. 189.
[9] S. Stagira, M. Zavelani-Rossi, M. Nisoli, S. De Silvestri, G. G. Lanzani, C. Zenz, P. Mataloni, and G. Leising, Appl. Phys. Lett. **73**, 2860 (1998).
[10] U. Lemmer, A. Haugeneder, C. Kallinger, and J. Feldmann, in *Semiconducting Polymers* (Ref. 8), p. 309.
[11] M. J. S. Dewar, E. G. Zoebisch, E. F. Healy, and J. J. P. Stewart, J. Am. Chem. Soc. **107**, 3902 (1985).
[12] AMPAC 5.0 User's Manual, © 1994 Semichem, 7128 Summit, Shwanee, KS 66216.
[13] E. Zojer *et al.* (unpublished).
[14] This CI active space is also consistent with the description obtained for the lowest-lying one-photon allowed state given in Table I.
[15] J. A. Pople, D. L. Beveridge, and P. A. Dobosh, J. Chem. Phys. **47**, 2026 (1967); J. Ridley and M. Zerner, Theor. Chim. Acta **32**, 111 (1973).

[16] R. J. Buenker and S. D. Peyerimhoff, Theor. Chim. Acta **35**, 33 (1974).

[17] In the approach used here, the one-photon excited states are in fact described at the single configuration interaction (SCI) level while the two-photon states are calculated by considering single and double excitations and decoupling them to the Hartree-Fock solution.

[18] D. Beljonne, G. E. O'Keefe, P. J. Hamer, R. H. Friend, H. L. Anderson, and J. L. Brédas, J. Chem. Phys. **106**, 9439 (1997).

[19] S. Stagira, M. Nisoli, G. Cerullo, M. Zavelani-Rossi, S. De Silvestri, G. Lanzani, W. Graupner, and G. Leising, Chem. Phys. Lett. **289**, 205 (1998).

[20] The results displayed in Table I have been obtained for geometries optimized including only configurations characterized by excitations from the HOMO to the LUMO. Increasing the CI active space in the AM1/MECI calculations, or calculating the excited-state absorption using the ground-state geometry yields the same three-peak structure. The shift of the peak positions in all cases in smaller than 0.16 eV. The only significant difference is a larger relative intensity of the highest energy maximum compared to the results shown in Table I. Considering the very complex nature of the description of that excited state (see Table I), this is not unexpected.

[21] D. Beljonne *et al.* (unpublished).

[22] A. Pogantsch, G. Heimel and E. Zojer (unpublished).

[23] C. Silva, A. S. Dhoot, D. M. Russel, M. A. Stevens, A. C. Arias, J. D. MacKenzie, N. C. Greenham, and R. H. Friend, Phys. Rev. B **64**, 125211 (2001).

[24] S. L. Dexheimer, W. A. Vareka, D. Mittleman, A. Zettl, and C. V. Shank, Chem. Phys. Lett. **235**, 552 (1995).